Spatial Graphs for Intra-cranial Vascular Network Characterization, Generation, and Discrimination

Stephen R. Aylward [a,*] Julien Jomier [a] Elizabeth Bullitt [b]

[a] *Kitware, Inc., Albany, NY and Chapel Hill, NC*

[b] *Department of Surgery, The University of North Carolina at Chapel Hill, USA*

Abstract

Graph methods that summarize vasculature by its branching topology are not sufficient for the statistical characterization of a population of intra-cranial vascular networks. Intra-cranial vascular networks are typified by topological variations and long, wandering paths between branch points.

We present a graph-based representation, called spatial graphs, that captures both the branching patterns and the spatial locations of vascular networks. Furthermore, we present companion methods that allow spatial graphs to (1) statistically characterize populations of vascular networks, (2) generate the central vascular network of a population of vascular networks, and (3) distinguish between populations of vascular networks. We evaluate spatial graphs by using them to distinguish the gender and handedness of individuals based on their intra-cranial vascular networks.

Key words: Vessel, Path, Atlas, Mental disorder diagnosis, Handedness, Gender

1 Introduction

Intra-cranial vasculature varies across individuals to such an extent that only a few of the largest intra-cranial vessels are sufficiently consistent to be depicted and labeled in anatomical atlases [19]. Variations in the location and connectivity of even those named vessels are common in a healthy population

* Corresponding Author. Email: Stephen.Aylward@Kitware.com. Address: 28 Corporation Drive Suite 204, Clifton Park, NY 12065 USA. Phone: (518) 371-3971.

[1] This work was funded in-part by NIH/NIBIB R01-EB000219 and NIH/NIHLB R01-HL069808

[3]. Furthermore, between branchpoints, intra-cranial vessels will often follow long and wandering walks. These walks must be preserved to truly capture the form and function (filling regions, etc.) of intra-cranial vasculature.

Our interest in characterizing intra-cranial vasculature arises from the mounting evidence that a genetic relationship exists between mental disorders and vascular network formation. It has been established that during development vascular endothelial growth factors (VEGF) not only spur vessel and tissue growth but also direct tissue differentiation and the formation of organs [16,17,14]. Furthermore, mutation of genes associated with controlling VEGF and blood vessel development have been correlated with a variety of mental disorders, including unexplained mental retardation [22], Down syndrome [12], and DiGeorge syndrome [21]. Motivated by these genetic correlations, we have been seeking a tool to quantify intra-cranial vascular network variations between individuals and populations. The hope is that such a tool would lead to the discovery of novel methods for the early detection, quantification, and treatment of mental disorders.

Our research has led to the development of a graph-theoretic method for representing and analyzing the intra-cranial vascular networks of individuals and populations. These "spatial graphs" capture the anatomical locations, branching patterns, and tortuous paths of intra-cranial vascular networks. Spatial graph formation begins with a centroid voronoi tessellation (CVT) [13] of intra-cranial space. Those CVT regions are potential nodes of a spatial graph. A vascular network, overlaid on a voronoi tessellation of space, defines a spatial graph by recording the branching sequence of CVT nodes visited by the network. These branching sequences can be equivalently recorded as weighted, asymmetric adjacency matrices. Adjacency matrix and node-specific statistics, such as the centrality [4] and branch probability at each node, can be collected for a population of vascular networks. These statistics can be used to probabilistically generate vascular networks that are central to a population. These statistics can be used to compute membership scores for an individual's vascular network. Membership scores from different population-specific graphs and be used to classify an individual.

Forming graph representations of vascular networks is not a new concept. In 1993 Dr. Gerig presented [11] an intra-cranial vessel segmentation technique and illustrated the reduction of those segmentations to graphs that represent their topology. Such branch-based graphs are the basis of much of the vessel-based liver lobe and heart vessel segmentation work being conducted in a variety of labs [10,20]. In computer-vision, graph theory has been applied to the characterization of the medial structure of objects [15]. To the best of our knowledge, a single method has not been previously demonstrated that applies graph theory to the characterization, the generation, and the discrimination of populations of intra-cranial vascular networks.

The next section presents the methods of spatial graphs. The subsequent section describes three evaluations of those methods: (1) visually assessing the central vascular network generated from the spatial graph statistics from right-handed males, (2) using male and female-specific spatial graphs of intra-cranial vasculature to determine the gender of testing individuals, and (3) using a right-handed-specific population graph to determine the handedness of testing individuals. In these evaluations, testing data did not overlap with the training data.

2 Methods

This section is divided into three subsections: forming spatial graphs, generating vascular networks from population-specific spatial graph statistics, and computing graph membership measures. While these method descriptions focus on intra-cranial vasculature, these methods are applicable to any branching, directed, possibly cyclic, space-occupying structure.

2.1 Forming Spatial Graphs

Spatial graph formation involves vessel extraction, inter-subject registration, space partitioning, and recording graph statistics. These steps are detailed next.

1) Extracting vascular networks from MRA data. Vascular network models must capture each vessel's location, blood-flow directions, and branchpoints to define a spatial graph. We have developed vessel network modeling methods that have been shown to produce accurate centerline and radius estimates [2] as well as accurate estimates flow direction and branch point location from time-of-flight MRA [5]. The details our as follows.

The vessel extraction technique estimates centerlines using dynamic-scale ridge traversal [9,1] and then estimates radii along the centerlines by maximizing a medialness measure [18]. This technique has been shown to be insensitive to the operator, image noise, and imaging modality [2]. It can be used to model the intra-cranial vessels visible in a 0.5x0.5x0.8mm^3 voxel size time-of-flight MRA in about 25 minutes.

After vessel extraction, by further analyzing the MRA, the connectivity of the vessels can be determined. We have developed a method that estimates flow direction and branch point location from MRA with an accuracy that rivals the abilities of radiologists when they use MRA and digital subtraction angiograms

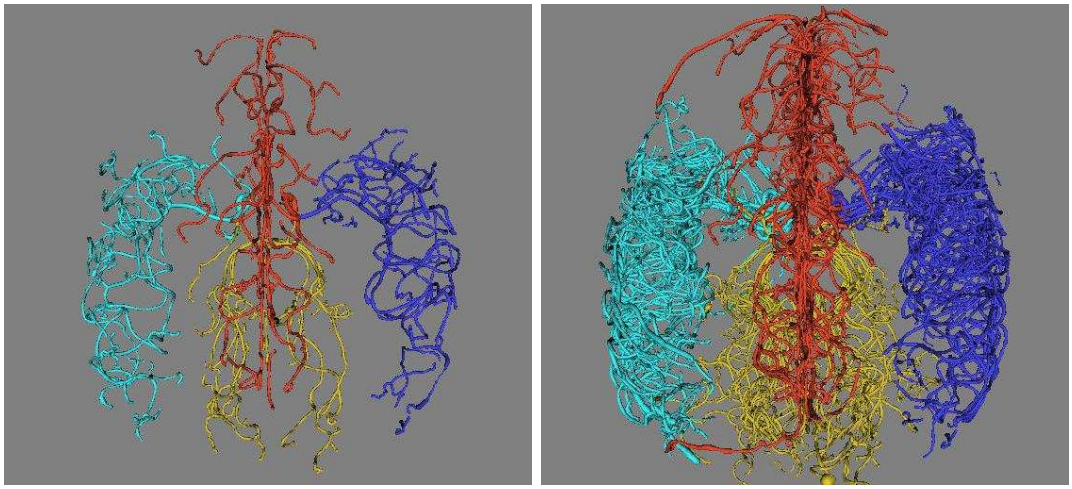

Fig. 1. *Right:* The intra-cranial, arterial network from a right-handed male, as captured by a time-of-flight MRA taken on a 3T system and as extracted and connected using the methods in this paper. *Left:* Aligned, intra-cranial, arterial networks from five right-handed males. Normal vascular variations are evident, daunting standard statistical analysis technques.

[5]. An example vascular network model from an individual's MRA is showing in Fig. 1. To compare such vascular network models between individuals, their networks must be aligned, as explained next.

2) Aligning individuals' vascular networks with a common coordinate frame. Vascular networks from MRA images are aligned by (a) rigidly registering the individuals' MRA to their T1 images; (b) performing an affine registration between the T1 images and the BrainWeb T1 atlas [8]; (c) composing the corresponding MRA-to-T1 and T1-to-atlas transforms; and (d) applying the composed transform to the extracted vessels. More details are available in [7]. In the work presented in this paper, alignment was quantified using the mutual information metric. Registration optimization was initialized using the centers of mass of the images and was refined using Brent line-search along gradient directions until convergence, defined by a minimum parameter change threshold. The aligned vascular networks from five right handed males are shown in Fig. 1. With the networks aligned, the next task is to produce a compact representation of their information.

3) Partitioning intra-cranial space into informative regions. The goal of this step is to partition the space occupied by the aligned vascular networks so that each region in the partition is equally likely to provide information about the vessels in each vascular network. A basic condition for such a partitioning is acheived when each region is equally likely to contain a portion of a vessel in every network. This concept led to the definition of a vascular density image that is inversely related to the expected distance to the nearest vessel. Partitioning a vascular density image into regions of equal integrated density

produces regions with equal likelihood of containing a vessel. The details are as follows.

An expected vascular density image is computed from a sample of aligned vascular networks [7]. Specifically, for each vascular network in the sample, the squared distance to the nearest vessel is computed throughout intra-cranial space and stored as a distance image. Each distance image is then inverted and normalized so that the value at each voxel is related to the likelihood of finding a vessel at that point. An expected vascular density image is defined as the voxel-by-voxel average of those inverted images. A voxel that contained a vessel in every network would have the highest intensity in the expected vascular density image, while a voxel that was never near a vessel in a network would have a value near zero. Similarly, the sum of the voxel intensities within a region of a vascular density image is correlated with the likelihood that the region contains a vessel. This property drove the selection of a partitioning algorithm, as described next.

The expected vascular density image is partitioned using the centroid voronoi tessellation (CVT) algorithm [13]. For this paper, 1,000 CVT regions are resolved using a probabilistic version of Lloyd's method [13]. First, the initial CVT regions are specified by randomly selecting 1,000 locations that span the vascular density image. These initial locations serve as region centers that define a tesallation of the image. Second, that tessallation is refined using a variant of k-means clustering in which the region centers are the means being adjusted. That is, the tessalation is iteratively refined by (a) generating a random sample of points using the density image as the probability density function, and then (b) updating the positions of the region centers to improve the regions' equi-probable covering of those random points. For the results in this paper, the tessallations were refined using 1,000 iterations with 100,000 new, random points per iteration. The procedure for generating random points from the density images and other details regarding the CVT algorithm are given in [13]. Results are illustrated in Fig. 2.

The regions of a partitioned vascular density image define the nodes that are linked in a spatial graph to encode the vessels in a vascular network. Methods for collecting path and branch statistics from multiple spatial graphs are given next.

4) Recording graph statistics. An adjacency matrix with node-specific statistics summarizes how one or more vascular networks map onto the CVT regions. Define v_k as the number of vessels in vascular network k, and ν as the number of vascular networks in a sample from population Ψ.

An adjacency matrix A_Ψ encodes the expected paths of the vessels in the vascular networks from population Ψ. Speficially, for vascular networks $k =$

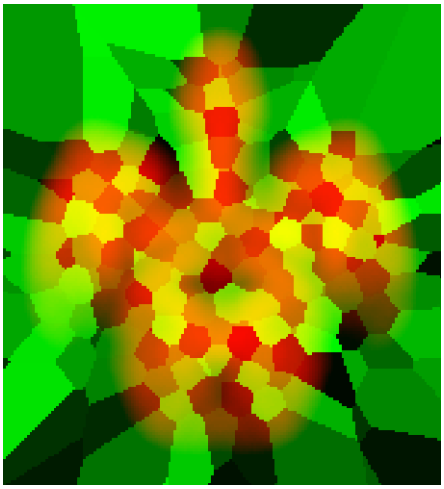

Fig. 2. An axial slice (at the level of the Circle of Willis) through the mean vessel distance map and CVT partitioning formed from 18 individuals. The fuzzy (red) object in the background is the expected vascular density. The crisp (green) overlay uses random intensities to depict the computed CVT regions.

$1..\nu$, as each vessel's flow-directed path crosses from CVT region i to CVT region j, the corresponding position $A_\Psi(i,j)$ is increased by $1/(v_k * \nu)$. This weighting compensates for level-of-detail variations in the vascular networks; if more vessels are included in a network, then the weight given to any single adjacency pair is reduced.

Population specific statistics regarding the vessels that pass through each CVT region are also recorded. These node statistics summarize local and connectivity information. Specifically, for all vascular networks $k = 1..\nu$, at each CVT region we record (a) the number of times it contains a branch point, (b) the mean radius of the vessel points that are contained within it, and (c) the number of times a root artery, e.g., a carotid or basilar artery, originates from within it. Additionally, we compute node centrality as a local summary of connectivity.

The concept of network node centrality was introduced by sociologists to determine the "popular people" in a social network, i.e., the most "central person" in directed communications [4]. For a person i in a social network, define e_i as the externally defined social status of the person. A parameter α weights the influence of that external status on internal exchanges. The centrality c_i of a person i is then computed as

$$c = (I - \alpha A^t)^{-1} e \tag{1}$$

where A is the asymmetric adjacency matrix and I is the identity matrix.

In a spatial graph that represents a vascular network, node centrality estimates

the size of the sub-network that follows from that node. For example, the CVT regions containing the carotid arteries would have higher centrality values than more distal regions. To achieve this measure, every CVT node i was given equal external status, i.e., $e_i = 1$ for all i. Additionally, α was set to 0.01 to reduce the influence of each node's external status relative to the cummulative status of the nodes that communicate with it. To direct communications along a graph to be towards its carotids' nodes, the transpose of A was remove from Equ 1 to reverse the link directions in the spatial graphs. Via this formulation, centrality values can be computed using a populations adjacency statistics A_Ψ. Using populations' adjacency and node statistics, vascular graphs can be generated and classified, as described next.

2.2 Generating Central Vascular Networks

Generating a vascular network from a population's spatial graph can be accomplished by a greedy traversal of the population's adjacency matrix and the consideration of the branch probabilities at its nodes. Since each node corresponds to a volume in space, a branching sequence of nodes defines a branching network passing through space. Two user specified threshold values control the generation process. The first threshold θ_A indicates the minimum level of adjacency required for a vessel traversal to continue. The second threshold θ_B indicates the minimum branch-support required for a branch point to be taken. Define the vector b_i as the probability of branching at node i for population Ψ. The branch-support $B(i, j)$ from a node i to node j is then defined via $B = Ab$.

Generation begins at the node that most often contained a root (carotid) vessel, as reported by the recorded node statistics. The largest weighted adjacency from that node is then chosen as the next transition in the generated graph. Adjacent nodes, not selected for continued generation, are searched for branch-support values above θ_B. If a branch node is found, it is queued for generation after the current vessel's generation terminates. A vessel's generation terminates when it encounters a node from which none of the adjacent nodes have an adjacency value above θ_A. Future research should consider statistics regarding radius, mean curvature, etc. when generating vessels.

2.3 Graph Membership Measures

Membership scores for a new vascular network, represented by the spatial graph g, are conditional on a population Ψ's spatial graph G_Ψ. We evaluate two membership scores in this paper: $\Sigma_A(g|G_\Psi)$ is the sum of the adjacency weights in G_Ψ for all transitions that also exist in g, and $\Sigma_c(g|G_\Psi)$ is the sum of

the centrality values for the CVT nodes in G_Ψ that are also involved in g. Both of these values should be maximized when a vascular network is compared with a graph that represents the population to which that vascular networks belongs. The next section describes experiments which test this theory.

3 Results

Three experiments were conducted to evaluate spatial graphs. Each of these is a challenging problem in medical image analysis.

For these experiments, MRA and T1-weighted MR images were collected on a Siemens Allegra head-only 3T MR system. MRA data was acquired using a time-of-flight sequence at 0.5x0.5x0.8mm^3 voxel spacing. T1-weighted MR data was acquired at 1x1x1mm^3.

The images from an individual were either used for training or testing, but never for both. Individuals were labeled by gender and self-reported handedness.

All of the experiments began with a common CVT partitioning of intracranial space. Specifically, vascular networks from 16 training-data, right-handed males (4 age 20-29, 5 age 30-39, 7 age 40-44) and 18 training-data, right-handed females (8 age 20-29, 5 age 30-39, 5 age 40-44) were combined to produce a common mean density map. The CVT of that map was computed once. Adjacency matrices, node centrality, and other measures were computed using the designated individuals' vascular networks combined with this common CVT partitioning. Using a common CVT partitioning may have reduced sensitivity and specificity, but it simplified comparisons across the populations' spatial graphs. This CVT partitioning is depicted in Fig. 2.

3.1 Experiment 1: Vascular Graph Generation

The first experiment demonstrates the generation of a vascular network for right-handed males. Using the 16 training-data, right-handed males, a right-handed, male population spatial graph was computed. The vascular network generation method described above was then applied. Threshold values were chosen iteratively to produce realistic looking results, $theta_A = 0.001$ and $\theta_B = 0.001$ - in the future, these thresholds can be derived from population statistics. For visualization, the mid-points on the lines between the centroids of each generated sequence of nodes were used as the control points for a b-spline curve through space. A constant radius of 0.5 mm was used for visualizing the

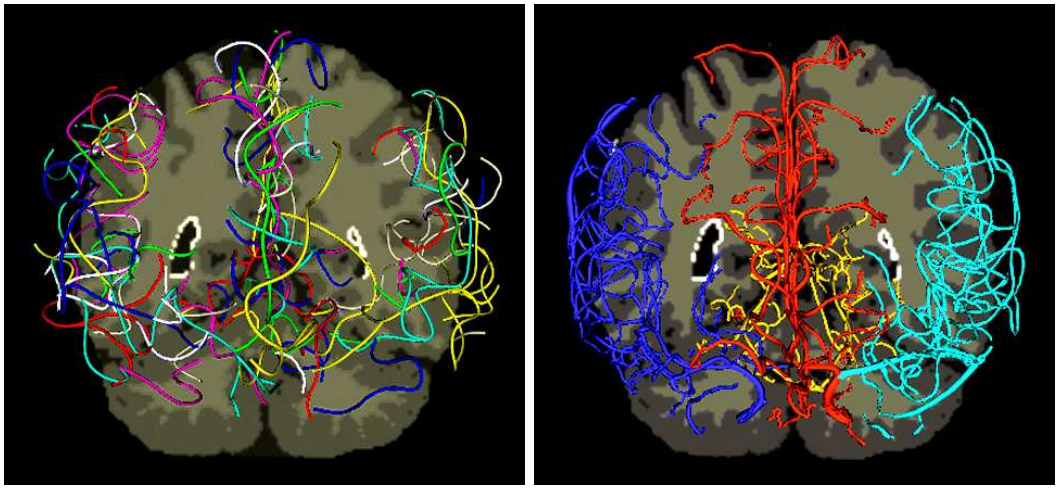

Fig. 3. Left: A vascular network generated from the right-handed male graph. Right: A vascular network from one of the training right-handed males. Carotids, circle of willis, vascular groups, other vascular patters are evident in the generated network.

vessels as tubes.

The generated central vascular network is visualized in Fig. 3. Subjectively, there are striking similarities between the generated and actual intra-cranial vascular networks. The generation method's threshold values can be manipulated to produce various levels of branching detail. Major vascular groups, the carotids, circle of willis, basilar artery, communicating arteries, and other major vessels are evident. Using b-splines to visualize the node adjacency sequence may have exaggerated intra-node vessel curvature.

3.2 Experiment 2: Distinguishing Gender

The second experiment involved distinguishing males from females based on intra-cranial vasculature. Two population-specific spatial graphs were computed: one using the 16 training-data, right-handed males and the other using the 18 training-data, right-handed females. For each population-specific graph, the membership measures $\Sigma_A(g|G_\Psi)$ and $\Sigma_c(g|G_\Psi)$ were computed for 5 testing-data, right-handed males (2 age 20-29 and 3 age 30-39) and 6 testing-data, right-handed females (1 age 20-29, 2 age 30-39, 3 age 40-49).

Gender classification results are shown in Tbl. 1. The success of Σ_A and failure of Σ_c implies that gender differences are not based on the location or number of vessels, but it is the directed vascular paths throught space that distinguish males from females. Further research is focusing on visualizing these differences.

Table 1
Confusion matricies for gender classification using the integrated adjacency and integrated centrality measures.

$\Sigma_A(g\|G_\Psi)$		Assigned Label	
		Male	Female
Truth	Males	4	1
	Females		6

$\Sigma_c(g\|G_\Psi)$		Assigned Label	
		Male	Female
Truth	Males	5	
	Females	3	3

Table 2
Confusion matricies for handedness classification using the integrated adjacency and integrated centrality measures. Handedness is self reported. Spatial graph for representing the left-handed population was defined by flipping the right-handed spatial graph about its mid-sagittal plane.

$\Sigma_A(g\|G_\Psi)$		Assigned Label	
		Right Handed	Left (mirrored-right) Handed
Truth	Right Handed	3	
	Left Handed		3

$\Sigma_c(g\|G_\Psi)$		Assigned Label	
		Right Handed	Left (mirrored-right) Handed
Truth	Right Handed	1	2
	Left Handed	2	1

3.3 Experiment 3: Determining Handedness

Our third experiment involved analyzing brain lateralization to determine the self-reported handedness of individuals. To study brain lateralization, instead of creating a population-specific spatial graph for left-handed males, we mirrored the right-handed graph along its x-axis. This mirroring approximates brain lateralization since the BrainWeb atlas' mid-sagittal plane is at the center of and normal to the x-axis. Using these right-handed male and mirrored-right-handed-male spatial graphs, membership measures $\Sigma_A(g|G_\Psi)$ and $\Sigma_c(g|G_\Psi)$ were computed for the 3 testing-data right-handed males and

for 3 testing-data left-handed males (ages 19, 26, and 29).

Results from handedness classification using intra-cranial vasculature are shown in Tbl. 2. Again the adjacency membership measure $\Sigma_A(g|G_\Psi)$ lead to correct labels for all testing-data individuals. The centrality measure $\Sigma_c(g|G_\Psi)$ had a 66% classification error. Again, the success of $\Sigma_A(g|G_\Psi)$ and the failure of $\Sigma_c(g|G_\Psi)$ suggests that the direct paths of intra-cranial vasculature is key to distinguishing these populations.

4 Discussion

We have developed spatial graphs as a technique which is well suited for characterizing intra-cranial vasculature. Initial results indicate that spatial graphs can be used to classify the gender and handedness of individuals. These successes suggests that spatial graphs can be used to study the genetic relationship that may exists between mental disorders and vascular network formation [12,21].

One particularly interesting finding is that when various membership measures are compared, classification experiments suggest that it is the paths taken by the vessels in a network (their adjacency matrices), not their centrality, that distinguishes genetic vascular variations.

While these results are encouraging, we are very cautious about drawing any conclusions beyond the limited data involved. It is critical that these methods be applied to larger datasets before suggesting that any general "truths" have been revealed. Future work will also pursue more advanced statistical analysis techniques.

References

[1] Aylward, S; Pizer, S; Eberly, D; Bullitt, E, *Intensity Ridge and Widths for Tubular Object Segmentation and Description*, MMBIA '96: Proceedings of the 1996 Workshop on Mathematical Methods in Biomedical Image Analysis, pp. 131, 1996

[2] Aylward, S; Bullitt, E, *Initialization, Noise, Singularities and Scale in Height Ridge Traversal for Tubular Object Centerline Extraction*, IEEE TMI 21(2):61-75, 2002

[3] Baskaya, MF; et al. *Surgical and Angiographic Anatomy of the Posterior Communicating and Anterior Communicating Arteries*, Neuro-anatomy 3:38-42, 2004

[4] Bonacich, P; Lloyd, P, *Eigenvector-Like Measures of Centrality for Asymmetric Relations*, Social Networks 23:191-201, 2001

[5] Bullitt, E; Aylward, S; Liu, A; Stone, J; Mukherji, S; Coffey, C; Gerig, G; Pizer, SM, *3D Graph Description of the Intracerebral Vasculature from Segmented MRA and Tests of Accuracy by Comparison with X-Ray Angiograms*, IPMI:308-321, 1999

[6] Bullitt, E; Aylward, S; Smith, K; Mukherji, S; Jiroutek, M; and Muller, K, *Symbolic Description of Intracerebral Vessels Segmented From MRA and Evaluation by Comparison with X-Ray Angiograms*, MedIA 5:157-169, 2001

[7] Chillet, D; Jomier, J; Cool, D; Aylward, S, *Vascular Atlas Formation Using a Vessel-to-Image Affine Registration Method*, MICCAI :335-342, 2003

[8] Cocosco, CA; Kollokian, V; Kwan, RK-S; Evans, AC, *BrainWeb: Online Interface to a 3D MRI Simulated Brain Database* NeuroImage 5(4), 1997

[9] Eberly, D; *Ridges in Image and Data Analysis*, Series on Computational Imaging and Vision, Kluwer Academic Publishers, September, 1996

[10] Ezquerra, N; Capell, S; Klein, L; Duijves, P, *Model-Guided Labeling of Coronoary Structure*, IEEE TMI 17(3):429-441, 1989

[11] Gerig, G; Koller, T; Székely, G; rechbühler, C; übler, O, *Symbolic Description of 3-D Structures Applied to Cerebral Vessel Tree Obtained From MR Angiography Volume Data*, IPMI :94-111, 1993

[12] Hesser, BA; et. al, *Down Syndrome Critical Region Protein 1 (DSCR1), a Novel VEGF Target Gene That Regulates Expression of Inflammatory Markers on Activated Endothelial Cells*, Blood 104(1):149-158, 2004

[13] Ju, L; Du, Q; Gunzburger, M, *Porbabilistic Methods for Centroidal Voronoi Tessellations and Their Parallel implementations*, Parallel Computing 28:1477-1500, 2002

[14] Lammert, E; Cleaver, O; Melton D, *Induction of Pancreatic Differentiation by Signals from blood vessels*, Science 294:564-7, 2001

[15] Macrini, D; Shokoufandeh, A; Dickinson SJ; Siddiqi, K; Zucker; SW, *View-Based 3-D Object Recognition Using Shock Graphs*, ICPR:24-32, 2002

[16] Melton DA, *Blood Vessels Trigger Development of the Pancrease*, HHMI Bulletin, September, 2001

[17] Melton DA, *Blood Vessels Shape Organs*, Science Express, 160(13) September 29, 2001

[18] Morse, BS; Pizer, SM; Liu, A, *Multiscale Medial Analysis of Medical Images*, IPMI '93: Proceedings of the 13th International Conference on Information Processing in Medical Imaging, pp. 112–131, 1993

[19] Netter, F, *Atlas of Human Anatomy*, Novartis, East Hanover, New Jersey, Pages 525, 1989

[20] Selle, D; Preim, B; Schenk, A; Peitgen, H.-O., *Analysis of Vasculature for Liver Surgical Planning* IEEE TMI 21(11):1344-1357, 2002

[21] Stalmans, I; et al., *VEGF: A Modifier of the del22q11 (DiGeorge) Syndrome?* Nature Medicine 9:173-182, 2003

[22] Vervoort, VS; Beachem, MA; Edwards, PS; Ladd, S; Miller, KE; de Mollerat, X; Clarkson, K; DuPont, B; Schwartz, CE; Stevenson, RE; Boyd, E; Srivastava, AK; *Possible Gene for Form of Mental Retardation, Brain Development Identified" NIH News Release, June 27, 2002 Also in "AGTR2 Mutations in X-Linked Mental Retardation*, Science, 296(5577):2401-2403, 2002